Novel Tunable Peace-Logo Planar Metamaterial Unit-Cell for Millimeter-Wave Applications

Farzad Khajeh-Khalili and Mohammad Amin Honarvar

A novel class of planar metamaterial unit-cells consisting of a peace logo pattern is presented. A significant advantage of the proposed peace-logo planar metamaterial (PLPM) unit-cell over existing designs is its tunability, simplicity, and compatibility with microstrip structures. The theoretical analysis is founded on the famous transmission-line theory for the metamaterial concept. Then, the tunable dual-band two-sided PLPM (TSPLPM) unit-cell is designed by printing a similar PLPM pattern at the bottom of the substrate. The influence of the bottom PLPM pattern on the resonance frequencies of the unit-cell was analyzed by performing numerical simulations using CST Microwave Studio 2017 and HFSSv15 simulators. The results of the numerical simulations demonstrated that the proposed TSPLPM has the ability to control the resonance frequencies over 50 GHz–75 GHz for millimeter-wave applications.

Keywords: Metamaterial, Millimeter-waves, PLPM, Tunable, Unit-cell.

I. Introduction

In 1968, metamaterials were theoretically introduced as a new class of materials by Veselago [1]. However, it took three decades for the first metamaterial prototype to be realized [2]. Since the initial development of metamaterials, many configurations have been used as metamaterial unit-cells, such as split-ring resonators (SRRs), complementary split-ring resonators (CSRRs), and H- or S-shaped unit-cells [3]–[5].

Metamaterials are artificially produced materials that have electromagnetic attributes, and these structures are not usually found in nature. Several recent papers have reported the use of metamaterials that produce negative relative permittivity and permeability [6]–[9]. The miniaturization of metamaterial unit-cells is one of the important issues, especially at low frequencies. Different techniques have been used for the miniaturization of metamaterial unit-cells, such as using fractal and spiral resonators [10]–[12]. Recently, metamaterial structures have been used for beam-tilting, gain enhancement, and frequency and beam switching applications in microwave and millimeter-wave antennas [13]–[15]. In all of these cases, the main role of the metamaterial medium is to provide a refractive index that is different from the host medium when interacting with the incident electromagnetic wave. However, almost all of the conventional unit-cells possess a single-band metamaterial response. This issue becomes important when we want to use metamaterials in multi-band or wideband applications, such as beamforming or gain enhancement in all of the operating bandwidths of a multiband or wideband antenna. To solve this problem, various reconfigurable unit-cells are proposed [16]–[18]. However, they need to be implemented on a high-epsilon substrate. Moreover, reconfigurable unit-cells may be

Manuscript received Jan. 13, 2018; revised Mar. 12, 2018; accepted Apr. 10, 2018.

Farzad Khajeh-Khalili (khalili.farzad@gmail.com) and Mohammad Amin Honarvar (corresponding author, amin.honarvar@pel.iaun.ac.ir.com) are with the Department of Electrical Engineering, Najafabad Branch, Islamic Azad University, Najafabad, Iran.

lossy and very difficult to implement, especially at millimeter-waves. It should be noted that recently, tunable metasurfaces at different wavelengths, such as encoding graphene metasurfaces and tunable anomalous refraction based on graphene metasurfaces are reported in [19]–[21].

In this study, the peace-logo planar metamaterial (PLPM) unit-cell is first designed, and the permeability and permittivity of the effective constitutive parameters are adopted from the *S*-parameters. Then, the tunable dual-band two-sided PLPM (TSPLPM) unit-cell is designed by printing a similar PLPM pattern at the bottom of the substrate. The analysis is based on the transmission line theory (TLT) for metamaterial notion. According to the numerical simulation results obtained from CST Microwave Studio 2017 and HFSSv15, it has been proven that the TSPLPM shows a dual-band metamaterial behavior over the frequency range of 50 GHz–75 GHz for millimeter-wave applications. Finally, the performance of the TSPLPM unit-cell is compared to several other unit-cells. This comparison reveals that the proposed unit-cell can provide tunable resonances that are comparable to those of other designs.

II. PLPM Unit-Cell Design

1. Analysis of Transmission Line Theory

In this section, we perform a comprehensive review of how to design the proposed unit-cell. Figure 1 shows the geometry of the proposed PLPM unit-cell, which is based on a peace logo design. The peace logo is a universally employed attractive pattern used in the meetings of libertarians and peacekeepers. Actually, a peace logo can be realized as a planar metamaterial structure. Here, the proposed peace-logo unit-cell is designed on a Rogers RT5880 substrate with a relative permittivity of 2.2, tan δ = 0.0009, and with a thickness of h = 0.254 mm. The dimensions of the structure are: L_D = 6 mm, W_D = 5 mm, w = 0.2 mm, r = 2 mm, and θ = 135°.

As shown in Fig. 1, the peace logo design that is used here consists of a PEC circle without a gap, which is placed in the *xy* plane, as well as a PEC diameter along the *y*-axis, and two symmetrical radius lines relative to the *y*-axis, which are printed in the top of the substrate. The line-width and the dielectric constant of the substrate can be used to carefully control the frequency response of the PLPM unit-cell.

According to the analysis examined in [22], transmission line theory (TLT) can be occupied to depict the electromagnetic propagation behavior in this metamaterial structure It is clear that loss-less media can be demonstrated in terms of equivalent transmission line circuits. Figure 2 shows the equivalent circuit model of the proposed PLPM unit-cell. d is the length of the PLPM unit-cell, where d is small compared to the wavelength. This model is valid under the assumption that the size and distance between the adjacent radius lines are both electrically small. The medium exhibits passbands with a positive refractive index when ε_{eff} and μ_{eff} are simultaneously positive or when both of them are negative. From the TLT, if the series branch is capacitive, whereas the parallel branch is inductive, energy propagation takes place by backward waves, for which the phase velocity is against the energy velocity. In the same way, this is the region in which the propagation vector ($\vec{\beta}$) points in a direction that is inverse to the Poynting vector ($\vec{S}$). These propagating backward waves imply the presence of a negative refractive index [22]. Therefore, it becomes clear that the condition for obtaining a negative refractive index in the transmission line circuit of Fig. 1 is satisfied when the series branch is capacitive and the parallel branch is inductive.

Based on TLT, the inductance L^L_{PLPM} can be approximated by the magnetostatic inductance of a single PLPM pattern of width w and mean radius r, which is equal to the average radius of the conventional SRR that is presented in [2]. The value of L^L_{PLPM} inductor can be controlled by the radius r, width w, and angle θ. Each gap of the PLPM pattern contributes to global capacitance in

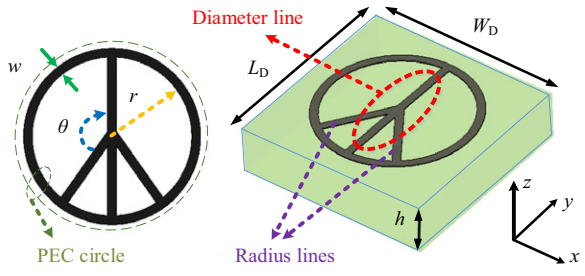

Fig. 1. Configuration of the proposed PLPM unit-cell.

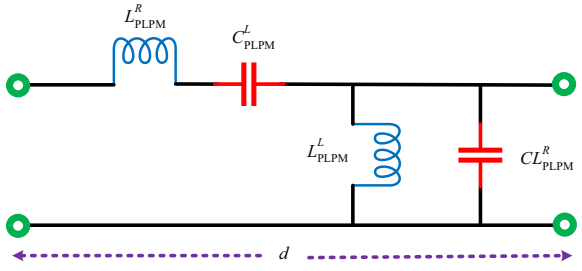

Fig. 2. Equivalent circuit model of the proposed PLPM unit-cell.

https://doi.org/10.4218/etrij.2018-0013

the form of a series connection of value C^L_{PLPM}. The capacitance C^L_{PLPM} is introduced for the entire capacity of the PLPM unit-cell.

Based on what is reported in [22], a purely left-handed unit-cell cannot exist physically. Therefore, the composite right- and left-handed (CRLH) model illustrates the most common metamaterial structure that is possible. The behavior of the CRLH model is completed by introducing the parasitic elements L^R_{PLPM} and C^R_{PLPM}.

In order to carry out the rigorous analysis of the proposed unit-cell, the propagation constant should be calculated. Therefore, the series and parallel resonance frequencies (f_S^{PLPM} and f_P^{PLPM}, respectively) are:

$$f_S^{\text{PLPM}} = \frac{1}{2\pi\sqrt{L^R_{\text{PLPM}}C^L_{\text{PLPM}}}}, \tag{1}$$

$$f_P^{\text{PLPM}} = \frac{1}{2\pi\sqrt{L^L_{\text{PLPM}}C^R_{\text{PLPM}}}}. \tag{2}$$

Now, based on the telegraphist's equations and some simplifications, the complex propagation constant is obtained for the PLPM LH range as:

$$\gamma = j\beta = -j\sqrt{\left(\frac{f}{f_R}\right)^2 \times \left(\frac{f_L}{f}\right)^2 - \sigma(2\pi f_L)^2}, \tag{3}$$

where f_R and f_L are respectively given by:

$$f_R = \frac{1}{2\pi\sqrt{L^R_{\text{PLPM}}C^R_{\text{PLPM}}}}, \tag{4}$$

$$f_L = \frac{1}{2\pi\sqrt{L^L_{\text{PLPM}}C^L_{\text{PLPM}}}}. \tag{5}$$

and variable σ is:

$$\sigma = L^R_{\text{PLPM}}C^L_{\text{PLPM}} + L^L_{\text{PLPM}}C^R_{\text{PLPM}}. \tag{6}$$

In the circuit model that is shown in Fig. 2, the lumped equivalents of the PLPM unit-cell are extracted as $L^R_{\text{PLPM}} = 56.27$ nH, $C^L_{\text{PLPM}} = 0.125$ fF, $L^L_{\text{PLPM}} = 312.6$ fF, and $C^R_{\text{PLPM}} = 22.51$ pF. Now, a typical diagram of the dispersion relation of (3) is depicted in Fig. 3. The PLPM unit-cell exhibits a frequency gap between f_S and f_P.

2. Numerical Outcomes and Discussion

In order to present a comprehensive numerical report and to validate the parameter extraction method and the obtained values of circuit elements, the PLPM unit-cell

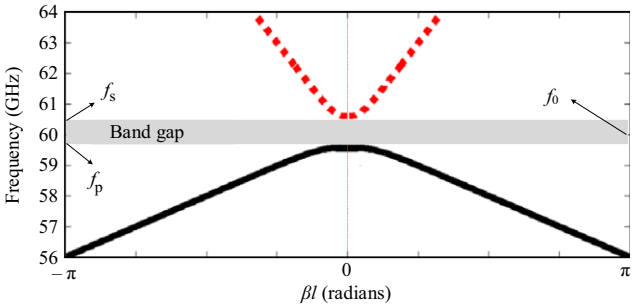

Fig. 3. Dispersion diagram for the proposed PLPM unit-cell.

is simulated using CST Microwave Studio 2017 and HFSSv15 simulators for an incident wave traveling along the positive x direction. Based on Fig. 1, PEC and PMC boundary conditions are used along the y and z directions, respectively, and two waveguide ports are located along the x direction. The S-parameters are illustrated in Fig. 4. According to Fig. 4, there is a resonance in S_{21} at 59.4 GHz. The simulated S-parameters are used in a standard extraction algorithm, and the real parts of the effective relative permeability and permittivity of the structure are calculated and plotted in Figs. 5(a) and 5 (b). According to the design equations in [23], the effective relative permeability and permittivity are adopted by using (7) and (8), where k_0 is the wave number and h is the substrate thickness.

$$\mu_r = \frac{2}{jk_0h}\frac{1-(S_{12}-S_{11})}{1+(S_{12}-S_{11})}, \tag{7}$$

$$\varepsilon_r = \frac{2}{jk_0h}\frac{1-(S_{11}+S_{12})}{1+(S_{11}+S_{12})}. \tag{8}$$

From Fig. 5, it can be observed that the magnitude of permeability is less than zero over the frequency range of 59.3 GHz–61 GHz. In addition, the magnitude of the permittivity is less than zero over the frequency ranges of 59 GHz–59.5 GHz and 59.7 GHz–60 GHz. In addition,

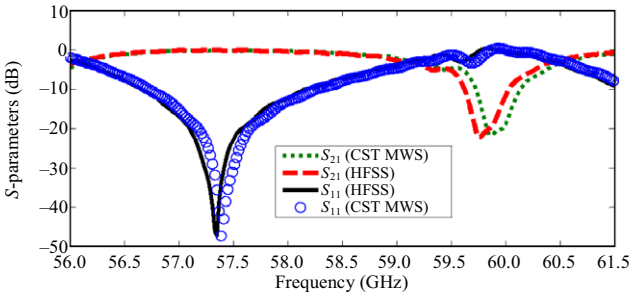

Fig. 4. S-parameters response of the proposed PLPM unit-cell.

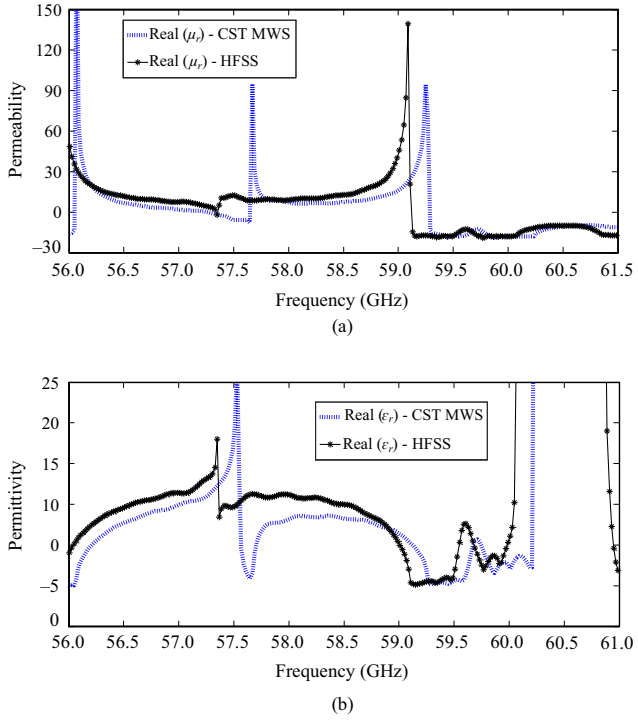

Fig. 5. Extracted (a) permeability and (b) permittivity of the PLPM unit-cell.

based on Figs. 3, 4, and 5, there is a good agreement between the theoretical and numerical results.

III. Tunable Two-Sided PLPM Design

In this section, in order to realize the proposed tunable unit-cell, the configuration shown in Fig. 6(a) is proposed. Based on Fig. 6(a), a new unit-cell is introduced using a PLPM pattern that is exactly the same as the previous structure at the bottom of the substrate. Based on what is introduced in Section II, the TLT can also be used for this unit-cell. The main advantage of the proposed unit-cell is that a frequency adjustment can only be achieved by rotating the PLPM pattern. Therefore, there is no change in the shape and size of the unit-cell. It should be noted that changing the microstrip structures for frequency tuning is a difficult task. According to Fig. 6(a), by rotating the bottom PLPM pattern at an angle of ψ, the coupling between the upper and lower PLPM patterns (C value) will change [24]. C accounts for the electric coupling between the upper and bottom PLPM patterns. Obviously, the resonance frequency of the TSPLPM will also change [24]. The balanced lumped element equivalent circuit model of the TSPLPM unit-cell is shown in Fig. 6(b). In this circuit model, the bottom PLPM is modeled by a tank resonator, which is exactly the same as the model PLPM unit-cell, and the

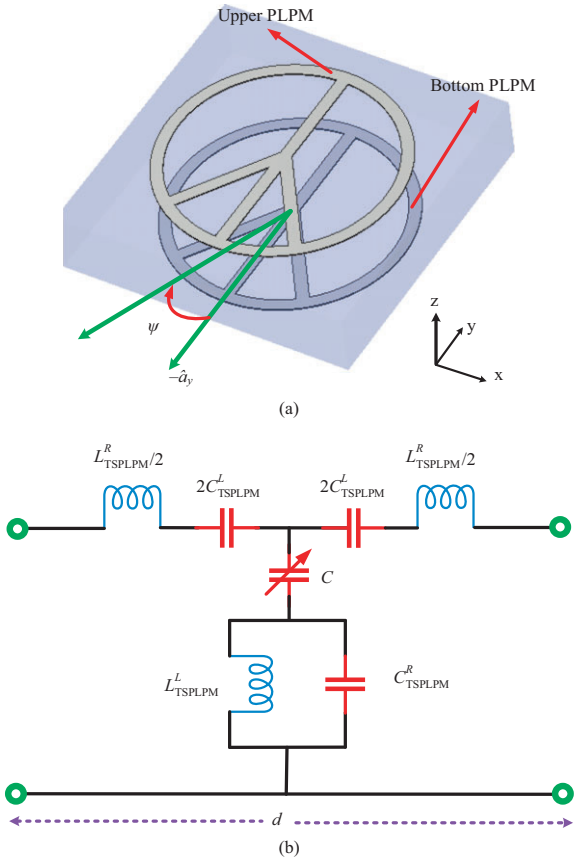

Fig. 6. Example of a TSPLPM unit-cell: (a) configuration and (b) equivalent circuit.

line inductance and capacitance are L^L_{TSPLPM} and C^L_{TSPLPM}, respectively. The parasitic elements are modeled by L^R_{TSPLPM} and C^R_{TSPLPM}.

The resonance frequency of the TSPLPM ($f_{\mathrm{S}}^{\mathrm{TSPLPM}}$) and the transmission-zero frequency ($f_{\mathrm{P}}^{\mathrm{TSPLPM}}$) at which the impedance of the parallel branch is equal to zero are obtained. At the resonance frequency of the TSPLPM:

$$f_{\mathrm{S}}^{\mathrm{TSPLPM}} = \frac{1}{2\pi\sqrt{L^R_{\mathrm{TSPLPM}} C^L_{\mathrm{TSPLPM}}}}. \tag{9}$$

The transmission zero frequency:

$$f_{\mathrm{P}}^{\mathrm{TSPLPM}} = \frac{1}{2\pi\sqrt{L^L_{\mathrm{TSPLPM}}(C + C^R_{\mathrm{TSPLPM}})}}. \tag{10}$$

For example, by considering the value of $\psi = 0°$, the S-parameters, permeability, and permittivity of the proposed TSPLPM are calculated, as shown in Fig. 7. According to Fig. 7(a), the proposed TSPLPM has a dual-band performance. The first and second resonance frequencies occur at 50 GHz and 60 GHz, respectively. The values of the permeability in the frequency bands (50 GHz–52 GHz and 57.5 GHz–62 GHz) are less than

https://doi.org/10.4218/etrij.2018-0013

zero, as shown in Fig. 7(b). According to Fig. 7(c), the permittivity also has the appropriate values in these frequency bands. This wide bandwidth is suitable for millimeter-wave applications. The lumped equivalents of the TSPLPM unit-cell for mentioned resonances are $L^R_{\text{TSPLPM}} = 51.03\,\text{nH}$, $C^L_{\text{TSPLPM}} = 0.202\,\text{fF}$, $L^L_{\text{TSPLPM}} = 1.02\,\text{nF}$, $C^R_{\text{TSPLPM}} = 66.11\,\text{pF}$, and $C = 19.60\,\text{pF}$.

Now, in order to better justify the proposed TSPLPM idea, 20 values are considered for the ψ angle, and are presented in Table 1. It should be noted that in order to obtain the most accurate solutions, two popular simulators, that is, CST Microwave Studio 2017 and HFSSv15, were used to perform simulations. For clarification regarding the different cases introduced for the ψ angle in Table 1, for example, the TSPLPM configurations of four angles (45°, 90°, 135°, and 180°) are shown in Fig. 8. In Table 1, for several values of ψ, S_{21} resonance frequencies and the fractional bandwidth (FBW) of each frequency band have been reported. It can be seen that by changing the ψ angle from 0° to 180°, the second S_{21} resonance frequency increases from 60 GHz to 75 GHz. However, the first S_{21} resonance frequency for the ψ angle changes is almost fixed. Therefore, the

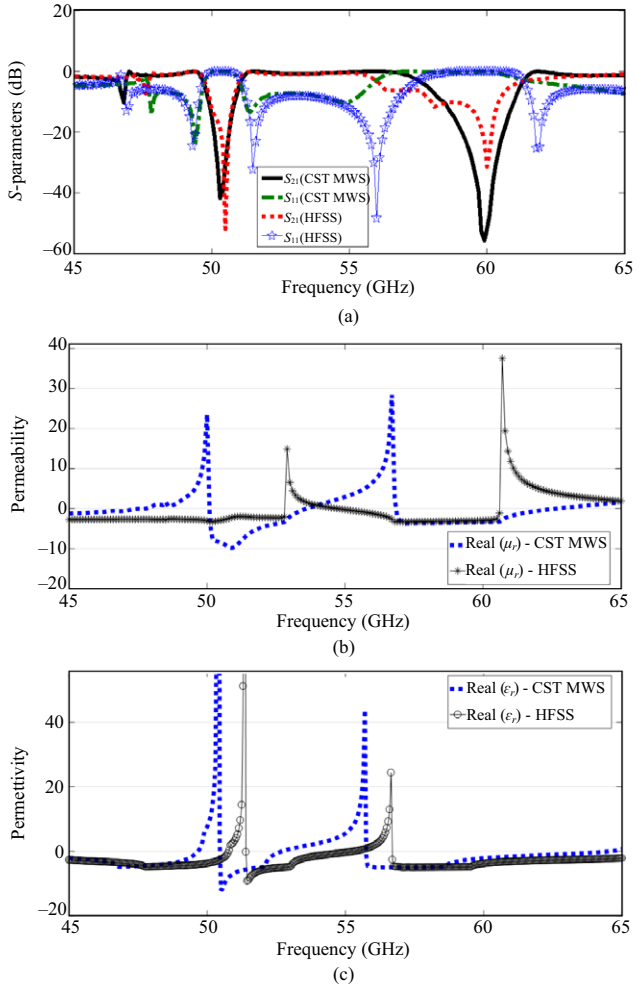

Fig. 7. Extracted parameters of the TSPLPM unit-cell: (a) S-parameters (S_{11} and S_{21}), (b) permeability, and (c) permittivity.

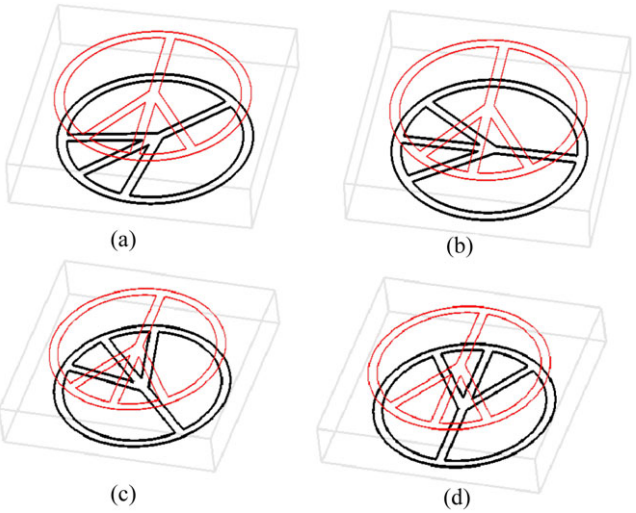

Fig. 8. Four cases of TSPLPM unit-cell: (a) $\psi = 45°$, (b) $\psi = 90°$, (c) $\psi = 135°$, and (d) $\psi = 180°$.

Table 1. Frequency responses (S_{21} resonances and FBW) for different angles with CST Microwave Studio 2017 and HFSSv15.

ψ (°)	S_{21} first resonance (GHz) (CST)	S_{21} second resonance (GHz) (CST)	FBW (%) 1st/2nd resonances (CST)	S_{21} first resonance (GHz) (HFSS)	S_{21} second resonance (GHz) (HFSS)	FBW (%) 1st/2nd resonances (HFSS)
0	50.36	60.04	1.84/4.24	50.50	60.88	1.68/6.35
45	50.44	65.93	2.82/4.73	50.10	65.76	2.72/5.79
90	50.76	68.92	3.23/3.55	50.80	70.21	2.11/3.60
135	50.72	70.67	3.19/4.15	51.10	73.20	2.44/4.62
180	50.76	75.08	3.70/5.31	50.81	76.20	2.48/6.75

proposed TSPLPM unit-cell has the ability to tune the resonance frequency over the entire frequency range of 50 GHz to 60 GHz for millimeter-wave applications. This can be observed in Fig. 9(a). It can be seen that there is a good proportion of the two full-wave simulators. However, the FBW of the first and second resonances, which is used to change the ψ angle from 0° to 180°, is reported in Fig. 9(b). According to Fig. 9(a), there is again a good fit proportion between the two simulators. To the best of the authors' knowledge, there have been no reports of unit-cells with this capability. We believe that the proposed unit-cell has the potential to use a millimeter-wave antenna to enhance the gain for other applications.

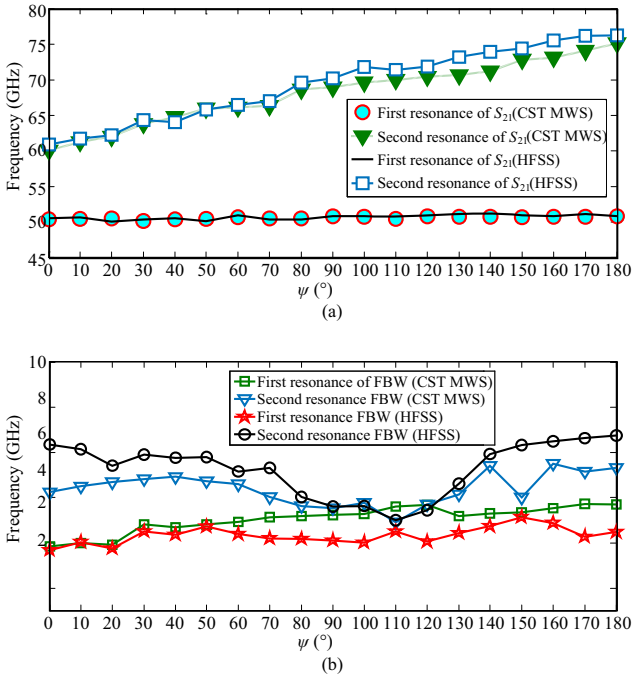

Fig. 9. Changes of resonance frequencies and FBW of TSPLPM unit-cell: (a) resonance frequencies and (b) FBW.

Table 2. Comparison of performance of this work with other unit-cells.

Ref.	Passbands	Frequency range (GHz)	Design method	Tunable
[5]	Single-band	54–57	H-shape	No
[13]	Single-band	50–53.5	Meander-line	No
[15]	Single-band	73–77	H-shape	No
This work	**Dual-band**	**50–75**	**PLPM**	**Yes**

This will be the next work of the authors. Finally, in Table 2, the proposed unit-cell is compared with several other metamaterial unit-cells. The tunable design and dual-band frequency response are among the benefits of the proposed unit-cell.

IV. Conclusion

In this study, a tunable metamaterial unit-cell was designed and simulated for the frequency band of 50 GHz to 75 GHz. This unit-cell is capable of providing two different resonance frequencies depending on the PLPM pattern rotations. This unit-cell can be used in gain enhancement, beam-switching, and beam-tilting applications for millimeter-wave antennas.

References

[1] V.G. Veselago, "The Electrodynamics of Substances with Simultaneously Negative Values of Permittivity and Permeability," *Soviet Phy. Uspekhi*, vol. 10, 1968, pp. 509–514.

[2] J.B. Pendry, A.J. Holden, D.J. Robbins, and W.J. Stewart, "Magnetism from Conductors and Enhanced Nonlinear Phenomena," *IEEE Trans. Microw. Theory Tech.*, vol. 47, no. 11, Nov. 1999, pp. 2075–2084.

[3] J. Choi, S. Oh, S. Jo, W.S. Yoon, and J. Lee, "Vertical Split Ring Resonator Using Vas with Wide Bandwidth and Small Electrical Size," *IEEE Microw. Wireless Compon. Lett.*, vol. 27, no. 1, Jan. 2017, pp. 16–18.

[4] C. Herrojo, F. Paredes, J. Mata-Contreras, S. Zuffanelli, and F. Martín, "Multistate Multiresonator Spectral Signature Barcodes Implemented by Means of S-Shaped Split Ring Resonators (S-SRRs)," *IEEE Trans. Microw. Theory Tech.*, vol. 65, no. 7, 2017, pp. 2341–2352.

[5] A. Dadgarpour, M. Sharifi Sorkherizi, A.A. Kishk, and T.A. Denidni, "Single-Element Antenna Loaded with Artificial Mu-Near-Zero Structure for 60 GHz MIMO Applications," *IEEE Trans. Antennas Propag.*, vol. 64, no. 12, Dec. 2016, pp. 5012–5019.

[6] D. Kim and J. Choi, "Novel Planar Metamaterial with a Negative Refractive Index," *ETRI J.*, vol. 31, no. 2, Apr. 2009, pp. 225–227.

[7] W. Tang, G. Goussetis, N.J.G. Fonseca, H. Legay, E. Sáenz, and P. de Maagt, "Coupled Split-Ring Resonator Circular Polarization Selective Surface," *IEEE Trans. Antennas Propag.*, vol. 65, no. 9, Sept. 2017, pp. 4664–4675.

[8] A. Dadgarpour, M.S. Sorkherizi, and A.A. Kishk, "High-Efficient Circularly Polarized Magnetoelectric Dipole Antenna for 5G Applications Using Dual-Polarized Split-

Ring Resonator Lens," *IEEE Trans. Antennas Propag.*, vol. 65, no. 8, Aug. 2017, pp. 4263–4267.

[9] A.R. Azad and A. Mohan, "Sixteenth-Mode Substrate Integrated Waveguide Bandpass Filter Loaded with Complementary Split-Ring Resonator," *Electron. Lett.*, vol. 53, no. 8, Apr. 2017, pp. 546–547.

[10] D. Wang, C. Aiu, and M. Hong, "Coupling Effect of Spiral-Shaped Terahertz Metamaterials for Tunable Electromagnetic Response," *Appl. Phys. A*, vol. 115, no. 1, Apr. 2014, pp. 25–29.

[11] F. Bilotti, A. Toscano, K.B. Alici, E. Ozbay, and L. Vegni, "Design of Miniaturized Narrowband Absorbers Based on Resonant-Magnetic Inclusions," *IEEE Trans. Electromagn. Compat.*, vol. 53, no. 1, Feb. 2011, pp. 63–72.

[12] V. Crnojevic-Bengin, V. Radonic, and B. Jokanovic, "Fractal Geometries of Complementary Split-Ring Resonators," *IEEE Trans. Microw. Theory Tech.*, vol. 56, no. 10, Oct. 2008, pp. 2312–2321.

[13] A. Dadgarpour, M.S. Sorkherizi, T.A. Denidni, and A.A. Kishk, "Passive Beam Switching and Dual-Beam Radiation Slot Antenna Loaded with ENZ Medium and Excited Through Ridge Gap Waveguide at Millimeter-Waves," *IEEE Trans. Antennas Propag.*, vol. 65, no. 1, Jan. 2017, pp. 92–102.

[14] I. Lim and S. Lim, "CPW-Fed Arbitrary Frequency-Switchable Antenna Using CRLH Transmission Line," *ETRI J.*, vol. 36, no. 1, Feb. 2014, pp. 151–154.

[15] A. Dadgarpour, B. Zarghooni, B.S. Virdee, and T.A. Denidni, "Improvement of Gain and Elevation Tilt Angle Using Metamaterial Loading for Millimeter-Wave Applications," *IEEE Antennas Wireless Propag. Lett.*, vol. 15, 2016, pp. 418–420.

[16] Z. Han, K. Kohno, H. Fujita, K. Hirakawa, and H. Toshiyoshi, "Tunable Terahertz Filter and Modulator Based on Electrostatic MEMS Reconfigurable SRR Array," *IEEE J. Sel. Top. Quantum Electron.*, vol. 21, no. 4, July/Aug. 2015, pp. 114–122.

[17] M. Ninic, B. Jokanovic, and P. Meyer, "Reconfigurable Multi-State Composite Split-Ring Resonators," *IEEE Microw. Wireless Compon. Lett.*, vol. 26, no. 4, Apr. 2016, pp. 267–269.

[18] A.K. Horestani, Z. Shaterian, J. Naqui, F. Martín, and C. Fumeaux, "Reconfigurable and Tunable S-Shaped Split-Ring Resonators and Application in Band-Notched UWB Antennas," *IEEE Trans. Antennas Propag.*, vol. 64, no. 9, Sept. 2016, pp. 3766–3776.

[19] J. Li et al., "Optical Polarization Encoding Using Graphene-Loaded Plasmonic Metasurfaces," *Adv. Opt. Mater.*, vol. 4, no. 1, Jan. 2016, pp. 91–98.

[20] T.-T. Kim et al., "Amplitude Modulation of Anomalously Refracted Terahertz Waves with Gated-Graphene Metasurfaces," *Adv. Opt. Mater.*, vol. 6, no. 1, Jan. 2018, pp. 1–7.

[21] Y. Niu, J. Wang, Z. Hu, and F. Zhang, "Tunable Plasmon-Induced Transparency with Graphene-Based T-shaped Array Metasurfaces," *Opt. Commun.*, vol. 416, no. 1, 2018, pp. 77–83.

[22] C. Caloz and T. Itoh, *Lectromagnetic Metamaterials: Transmission Line Theory and Microwave Applications*, Hoboken, NJ, USA: John Wiley & Sons, 2006.

[23] R. Marques, F. Mesa, J. Martel, and F. Medina, "Comparative Analysis of Edge- and Broadside-Coupled Split Ring Resonators for Metamaterial Design - Theory and Experiments," *IEEE Trans. Antennas Propag.*, vol. 51, no. 10, Oct. 2003, pp. 2572–2581.

[24] F. Khajeh-Khalili and M.A. Honarvar, "A Design of Triple Lines Wilkinson Power Divider for Application in Wireless Communication Systems," *J. Electromagn. Waves Appl.*, vol. 31, no. 16, Oct. 2016, pp. 2110–2124.

Farzad Khajeh-Khalili was born in Isfahan, Iran, in 1989. He received the M.Sc. degree with the highest honors in Telecommunication Engineering from the Islamic Azad University, Najafabad Branch, Iran in 2015. He is currently working toward the Ph.D. degree at the Islamic Azad University, Najafabad branch. His research interests include metamaterials, microwave devices, circuits, and subsystems.

Mohammad Amin Honarvar was born in Shiraz, Iran in 1982. He received his M.Sc. degree in Telecommunication Engineering from Shiraz University, Shiraz, Iran, in 2008, and his Ph.D. degree from the Science and Research branch, Islamic Azad University, Tehran, Iran, in 2012. Since 2012, he has been with the Department of Electrical Engineering, Najafabad Branch, Islamic Azad University, Iran, as an assistant Professor. His research interests include numerical methods in electromagnetics, as well as microwave circuits and component design.